Large Deformation Mechanical Behavior of Gelatin–Maltodextrin Composite Gels

VALERY NORMAND,* KEVIN P. PLUCKNETT, STEPHEN J. POMFRET, DUDLEY FERDINANDO, IAN T. NORTON

Unilever Research Colworth, Colworth House, Sharnbrook, Bedford, MK44 1LQ, United Kingdom

Received 29 February 2000; accepted 29 August 2000

ABSTRACT: The large deformation failure behavior of gelatin–maltodextrin composite gels was assessed. All the studied compositions were selected to lie within the incompatibility domain of the gelatin–maltodextrin phase diagram at 60°C, which produced gelatin continuous (maltodextrin included) and maltodextrin continuous (gelatin included) composites. Composite microstructural evaluation was performed using confocal laser scanning microscopy (CLSM). The large deformation mechanical behavior was measured in tension and compression experiments. Crack–microstructure interactions were investigated by dynamic experiments on the CLSM. The gelatin continuous composites exhibited pseudo-yielding behavior during tension and compression testing, and there was a significant decrease in modulus that arose from interfacial debonding. Conversely, the maltodextrin continuous composites exhibited an essentially brittle failure behavior, and there was an approximately linear increase in stress with increasing strain until fracture (which occurred at significantly lower strains than for the gelatin continuous composites). The CLSM observation of the failure of the notched samples also demonstrated interfacial debonding in the crack path; however, this occurred at significantly smaller strains than for the gelatin continuous samples with minimal elastic–plastic deformation of the maltodextrin matrix. The Poisson ratio was estimated to be close to 0.5 for these composites for all examined compositions. Compositions corresponding to a tie line of the phase diagram were also investigated to assess the influence of the relative phase volume (for constant phase compositions) on the failure behavior. The majority of the parameters subsequently extracted from the stress–strain curves were apparently functions of the individual phase volumes. © 2001 John Wiley & Sons, Inc. J Appl Polym Sci 82: 124–135, 2001

Key words: maltodextrin; fracture; biopolymer compatibility; interface

INTRODUCTION

The small deformation mechanical behavior for a gelatin (from lime hide, LH1)/maltodextrin (SA2) composite system has been extensively studied.[1–6] The purpose of the present work is primarily to assess the large deformation behavior of these materials. In particular, it is important to be able to relate failure properties and fracture propagation mechanisms to the composite microstructure. Preliminary observations were made on this system by Plucknett et al.[7] using confocal laser scanning microscopy (CLSM) and conventional dynamic tests where the gelatin-rich phase was the matrix of the composite.

Large deformation failure was studied by a number of authors for a range of biopolymer gels, which were structurally classified according to their different gelation mechanisms. These in-

Correspondence to: V. Normand (valery.normand@firmenich.com).

*Current address: V. Normand, Firmenich S.A., FFC, 7 Rue de la Bergère, 1217 Meyrin 2, Switzerland.

Journal of Applied Polymer Science, Vol. 82, 124–135 (2001)

clude networks based on polymer chains (e.g., gelatin), particle gels (e.g., casein), and gels of densely packed deformable particles (e.g., starch).[8] Several attempts were also made to characterize and model the failure behavior of composite gels containing rigid[9,10] and deformable particle inclusions.[11–13] These and other models typically assume either strongly or weakly bonded interface conditions between the filler particles and the matrix.

In the present study the mechanical response of gelatin–maltodextrin composite gels was determined in both tension and compression. The conventional dogbone-shaped samples and notched compact tension (CT) specimens were used for tension tests, and bulk cylindrical samples were used in the compression studies. Both of these types of test were also performed dynamically on a CSLM microscope to assess the influence of deformation on the gel structure. In particular, the CT technique was adopted to investigate microstructure–crack interactions. The influences of the continuous phase composition, including the particle size and phase volume, were investigated.

EXPERIMENTAL

Composite Fabrication

The gelatin was provided by SKW (Carentan, France) and was prepared by extraction from lime hide (LH1; PI = 4.7, M_n = 83,300 Da, polydispersity = 1.77, measured by GPC). Gelatin solutions were prepared by dissolving the powder at 60°C for 30 min in deionized water. To prevent bacteriological degradation of the protein, 500 ppm of sodium azide was added. Sirius red (500 ppm) was also added to all preparations to increase the fluorescence of the gelatin (i.e., for CLSM examination). When such solutions are cooled below 28°C, a 3-dimensional gel network appears in which the gelatin chains are linked by triple helices.

The maltodextrin (Paselli SA2) was provided by Avebe (Foxhol, The Netherlands). It is a polysaccharide biopolymer (a mixture of linear amylose and branched amylopectin) obtained after enzymatic degradation of potato starch[14] (M_n = 6.2 ± 0.5 10^5 Da, polydispersity = 1.45 ± 0.30, measured by light scattering). The solubilization of the maltodextrin was considered to be complete when the preparation was maintained at 98°C for a minimum of 30 min. Ordering occurs at temperatures below 31°C. The formation of the maltodextrin gel is strongly concentration and time dependent.[15] Maltodextrin is believed to form a gel of densely packed crystallite particles.

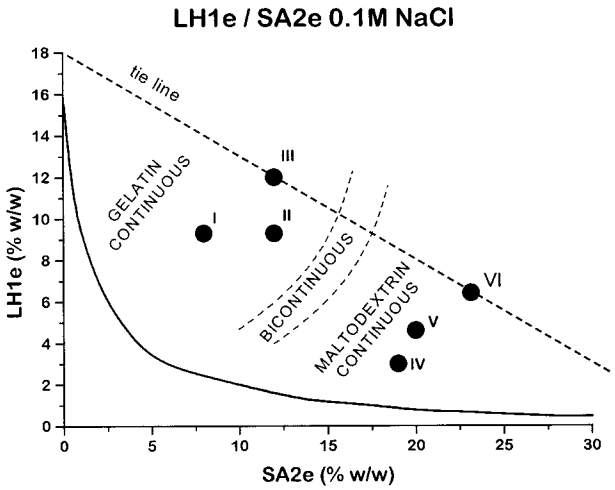

Figure 1 The phase diagram of the system of LH1e: SA2 in 0.1*M* NaCl solvent at 60°C.

The composite samples were prepared by mixing solutions of the two biopolymers at 60°C to achieve the overall compositions indicated in the phase diagram shown in Figure 1. All of the samples prepared in the current study were situated within the incompatibility domain of the gelatin–maltodextrin system.[5]

In order to examine the influence of the phase volume on the composite behavior (at constant phase composition), starting solutions for composite construction were prepared by mixing (in equal volumes) a 24% (w/w) gelatin solution with a 24% (w/w) maltodextrin solution at 60°C under light stirring for 5 min. This mixture was then stored at rest in a 60°C thermostat controlled oven to achieve phase equilibration. The gelatin-rich phase creamed, and the maltodextrin-rich phase sedimented. After 5 h at the equilibration temperature, two clear phases were observed. These phases were then decanted; by carefully weighing proportions for each phase, different final composites could be made with different phase volume ratios but identical phase compositions. In this procedure mixtures of the phases containing known phase volume fractions were homogenized for 5 min under strong stirring prior to gelation.

Tension Test Sample Preparation

Solutions prepared as above were subsequently poured between parallel glass plates (separated by 1.4-mm spacers and covered with hydrophobic paper to prevent the gelled solutions from sticking to the glass) preheated to 60°C in a water bath and protected from water contact by a plastic bag. The plates were then quenched rapidly to 9°C by immersion in a second water bath and stored for 24 h at 5°C.

Compression Test Sample Preparation

The solutions were poured into cylindrical molds (12.2-mm length and 12.5-mm diameter), the surface of which was previously covered by vacuum grease to prevent gel sticking. Samples were then rapidly cooled to 10°C to avoid large-scale phase separation.

Mechanical Testing and Microstructure Characterization

Compression and tensile tests were conducted using an Instron Universal testing machine (model 4501). Samples were equilibrated at 10°C prior to and during mechanical testing using a temperature controlled cabinet.

Tension Tests

A dogbone-shaped specimen geometry was chosen for the tensile tests, and samples were cut from the 1.4 mm thick gel sheets using a suitably shaped cookie cutter. The test specimens were then gripped on the Instron using double-sided tape. Only samples that failed within the gauge length were used for calculation of mechanical properties. Testing was conducted using a displacement rate of 50 mm/min. True failure stress (σ_t) and true failure strain (ϵ_t) was subsequently calculated using the following equations:

$$\sigma_t = \frac{F(L_0 + \Delta L)}{A_0 L_0} \tag{1}$$

$$\varepsilon_t = \ln\left(\frac{L_0 + \Delta L}{L_0}\right) \tag{2}$$

where F is the load, L_0 is the initial gauge length, ΔL is the displacement, and A_0 is the cross-sectional area.

Compression Tests

The compression tests made under lubricated conditions (dodecan) were also conducted at 50 mm/min. The true stress (σ_c) and true strain (ϵ_c) were calculated using the following equations:

$$\sigma_c = \frac{FH}{A_0 H_0} \tag{3}$$

$$\varepsilon_c = \ln\left(\frac{H}{H_0}\right) \tag{4}$$

where H_0 is the initial sample height and H is the sample height after deformation.

CLSM Characterization

The microstructures of the fabricated composites were assessed using a CLSM microscope. For the micrographs presented in this study the gelatin-rich phase was light in color while the maltodextrin-rich phase was dark, which was due to preferential staining of the gelatin by Sirius Red, which exhibits fluorescence under laser illumination. Large deformation mechanical tests, including observation of failure, were also performed on the CLSM microscope using a Minimat tension/compression testing stage. Two tension test geometries were utilized for these experiments: the conventional tensile test described above and a notched CT test. For the CT experiments the notched samples were subjected to small stepped tensile displacements (typically 0.1-mm steps at a displacement rate of 2 mm/min) while observing the notch tip on the CLSM. All CLSM visualization experiments were performed at 22 ± 1°C. It was generally observed that the notch eventually began to grow stably across the test specimen, after which further tensile displacements were generally unnecessary. Crack advance could then be followed directly on the CLSM microscope and recorded dynamically on video. In addition to the tension experiments, cylindrical samples were compressed between two lubricated glass plates and observed from above using the microscope to visually assess the deformation behavior in compression.

RESULTS AND DISCUSSION

Gelatin Continuous Composite Behavior

A typical set of Instron load–displacement curves, obtained for the gelatin continuous com-

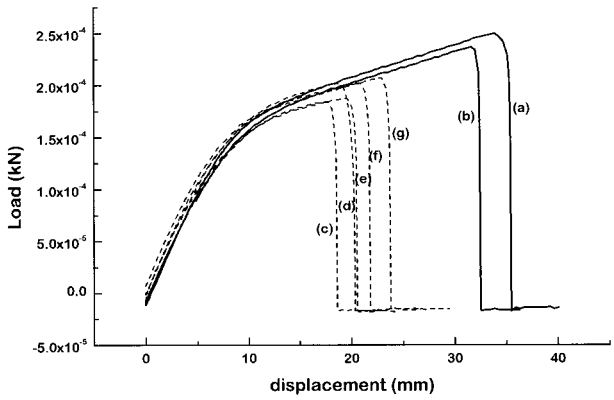

Figure 2 The tensile load–displacement curves obtained for composition III with rapid cooling (small inclusions, curves a and b) and slow cooling (large inclusions, curves c–g,).

position III (see Fig. 1) is shown in Figure 2. These observations were generally characteristic of gelatin continuous samples, and the large deformation failure curves showed three distinct regions.[7] The initial small displacement response (<5 mm displacement, equivalent to 8% true strain) corresponded to the linear elastic region with constant elastic modulus. This was followed by a region of decreasing elastic modulus with pseudo-ductile behavior and finally the sample fractures at large extensions (i.e., <50% strain).

Three different composite compositions were extensively investigated: composites I, II, and III were 8% SA2 and 9.3% LH1e, 12% SA2 and 9.3% LH1e, and 12% SA2 and 12% LH1e in 0.1*M* NaCl, respectively. The significant difference between these composites was the ratio of the stiffness of the included phase relative to that of the matrix. In composite system I the matrix modulus was higher than the particle modulus. In system II the particle and matrix moduli were similar, while in system III the modulus of the particles was larger than that of the matrix. A comparison of the composites in which gelatin was the continuous phase with pure gelatin behavior was already discussed in a preliminary article.[7]

It was apparent for these systems that the standard deviation error in the elastic modulus was small when compared to the error observed for the other failure properties. The elastic modulus can be viewed as a nominally intrinsic material property (dependent upon composition and processing and test conditions). However, the failure stress was largely dependent upon the largest flaw size and the flaw size distribution in any particular test specimen. For the immiscible phase-separated composites examined in the present study, the strength-controlling flaws were likely either large second phase particle inclusions, entrapped air bubbles, or surface and subsurface damaged regions caused by the specimen cutting procedure. This emphasized the strong influence of the microstructure on the large deformation behavior of such materials when compared to that in the linear viscoelastic small deformation region.

A CLSM image of the microstructure of composition I after failure is presented in Figure 3(a) and the edge of the fracture surface is shown on the right-hand side. The maltodextrin particle size was relatively small (10–20 μm), and the size distribution was not very broad. Evidence of residual strain was seen around the droplets of the included phase, mostly oriented in the direction normal to the fracture. The fracture surface was

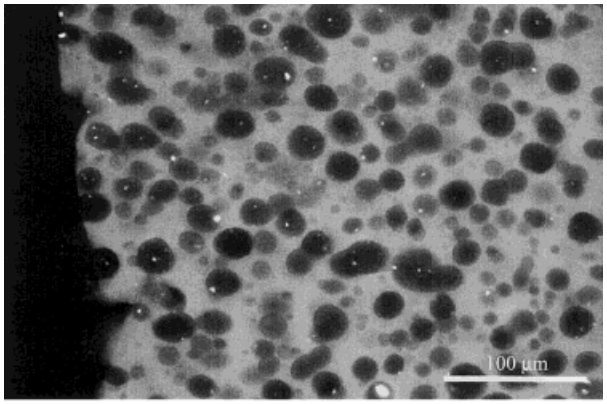

(a)

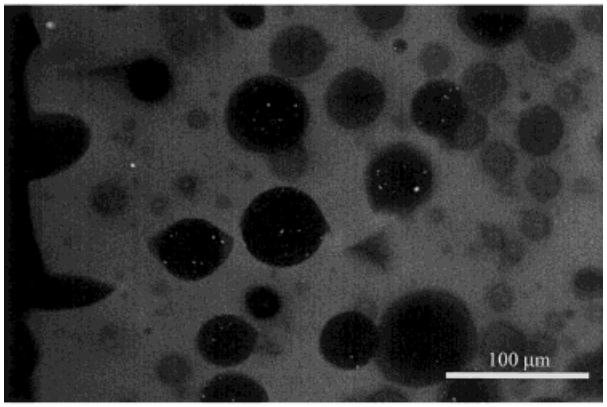

(b)

Figure 3 A CLSM microscope image of the edge of a fracture surface for compositions (a) I and (b) II (gelatin white, SA2 dark).

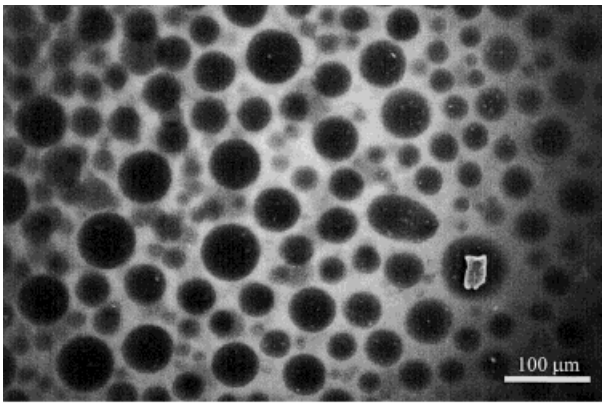

(a)

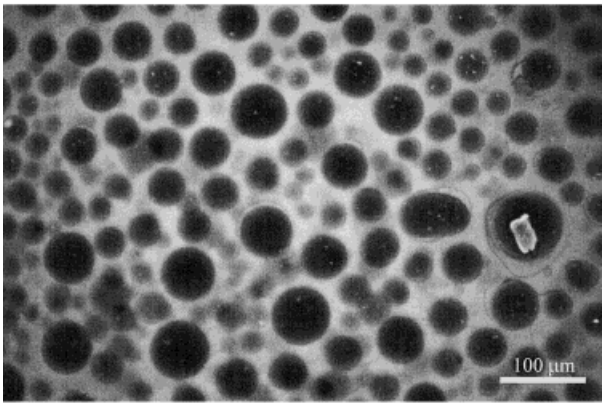

(b)

Figure 4 A CLSM image of the compression test under the microscope with (a) an uncompressed sample and (b) compressed at around 30% true strain.

irregular, debonding of SA2-rich particles was seen, and the particle shape remained intact on the fracture surface.

The microstructure of composition II after failure is shown in Figure 3(b). The particle size was generally larger than for composition I, as might be expected because of the higher SA2 phase volume in this sample, which promoted droplet coalescence. However, small particles were still seen (10 μm). The load–deflection behavior of this sample was shown in Figure 2. In Figure 3(b) interfacial debonding between the particle and the matrix is apparent, creating voids around the particle, predominantly in the direction of the applied strain. Qualitatively, only the largest particles exhibited this debonding behavior once the sample was relaxed after failure.

When the sample was cooled down at a higher rate, the maltodextrin particle size was significantly reduced for composition II (Fig. 2, curves a and b). It was notable that the initial elastic modulus, calculated in the linear elastic region of the load deflection curve, remained consistent for all samples, regardless of the included particle size (Fig. 2). A similar observation was reported by Brownsey et al.[13] for a gelatin-based system reinforced with Sephadex beads. However, although the modulus was essentially unchanged with a reduction in particle size, the failure load (stress) and displacement (strain) both increased dramatically (Fig. 2). Particle–matrix debonding was less apparent in the sample with smaller particle size (after failure and relaxation) as supported by earlier work.[16] In addition, the shape of the particles was qualitatively less spherical and they appeared to be stretched in the direction of the applied strain, which indicated a ratio of moduli close to 1 between the particle and the matrix.

Composition III exhibited tensile behavior similar to system II. Compression tests were also conducted under the CSLM microscope between two glass plates. These revealed that debonding occurred in the equatorial plane of the particle [Fig. 4(a,b)]. In this system debonding appeared at a larger strain than under applied tensile stress. For the large deformation tests (Fig. 5) the shape of the curve under compression was similar to that obtained under tension, exhibiting a linear response at low strain values (below 5%), then a ductile region, followed by fracture of the sample at large strains. However, the yield strain (i.e., strain at the onset of debonding) under compression was roughly twice the yield strain under tension. This behavior can be expected for an

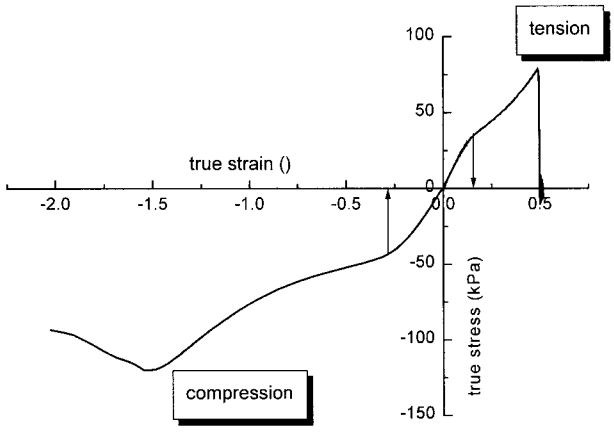

Figure 5 A comparison between tension and compression for system III (12% LH1e:12% SA2 in 0.1*M* NaCl solution). The true strain and stress were calculated according to eqs. (1)–(4).

incompressible material (i.e., Poisson ratio = 0.5) and the yield stress was roughly the same, which indicated that even under compression the failure was tension controlled. It was also noted that the fracture strain under compression was 2–3 times greater than that observed for tension. The Young's moduli measured in the early stages of the deformation process (i.e., strains $< 15\%$) were essentially identical for the tension and compression tests.

Maltodextrin Continuous Sample

The maltodextrin continuous samples exhibited a classical brittle failure response in tension[7] with a linear increase in displacement with increasing load, followed by sample failure. Clearly, the shape of the tensile curve was very different than that in the previous case (i.e., gelatin continuous) where pseudo-ductile behavior was noted.

Although the failure stresses for the maltodextrin continuous samples were comparable to those of the gelatin continuous materials, the failure strains were an order of magnitude lower, highlighting their brittle behavior, and linear elastic behavior occurred up to fracture.

The CLSM images of the microstructures of compositions IV and V after failure are shown in Figure 6(a,b). The gelatin inclusions were ~100 μm in diameter for compositions IV and V, and no obvious sign of particle percolation was noted.

In Figure 6(a) (composition IV) the fracture surface exhibits some distinct differences from the gelatin continuous samples. There are voids where a particle was detached, and the particle that remained with the sample appears to be unperturbed by the fracture path. The crack path goes around the particles (i.e., there is debonding), which again suggested that the interface between the maltodextrin matrix and the gelatin droplets was weak. However, although this behavior was somewhat similar to the gelatin continuous materials, it is clear that there was little or no particle–matrix debonding away from the actual crack, which was anticipated from the significantly lower failure strains observed for the maltodextrin continuous samples.

Figure 6(b) demonstrates a similar cross section of the fracture surface of composition V. It is apparent that once a gelatin droplet was partially pulled out from the matrix, it showed a residual (permanent) strain. This behavior was noted consistently for gelatin particles directly in the crack path; however, such *apparent* plastic deformation

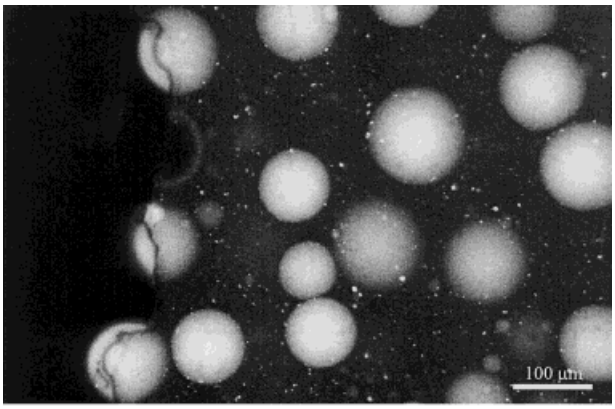

(a)

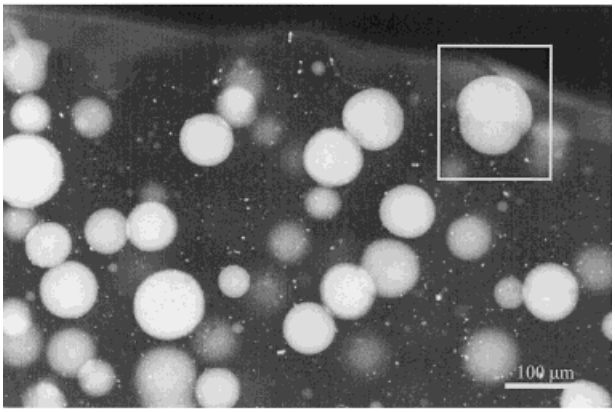

(b)

Figure 6 A CLSM image of the edge of a fracture surface for compositions (a) IV and (b) V (gelatin light inclusions, maltodextrin dark matrix). Residual strain can be observed in particles at the fracture surface.

was not observed away from the crack. Tensile fracture studies of pure monophase gelatin gels demonstrated that *apparent* unrecoverable plastic deformation can occur at high strains, which was attributed to structural alignment during straining.[17]

To further explain the fracture behavior of the maltodextrin continuous composites, notched CT tests were performed dynamically on the CLSM microscope using a Minimat stage. The results are presented in Figure 7 for composition IV; the same protocol was followed as adopted for a gelatin continuous sample discussed in Plucknett et al.[7] The displacement necessary to initiate crack growth from the original notch was 0.4 mm, which was significantly less than required for the gelatin continuous samples (several millimeters). It was readily apparent that the shape of the crack was considerably different than the gelatin

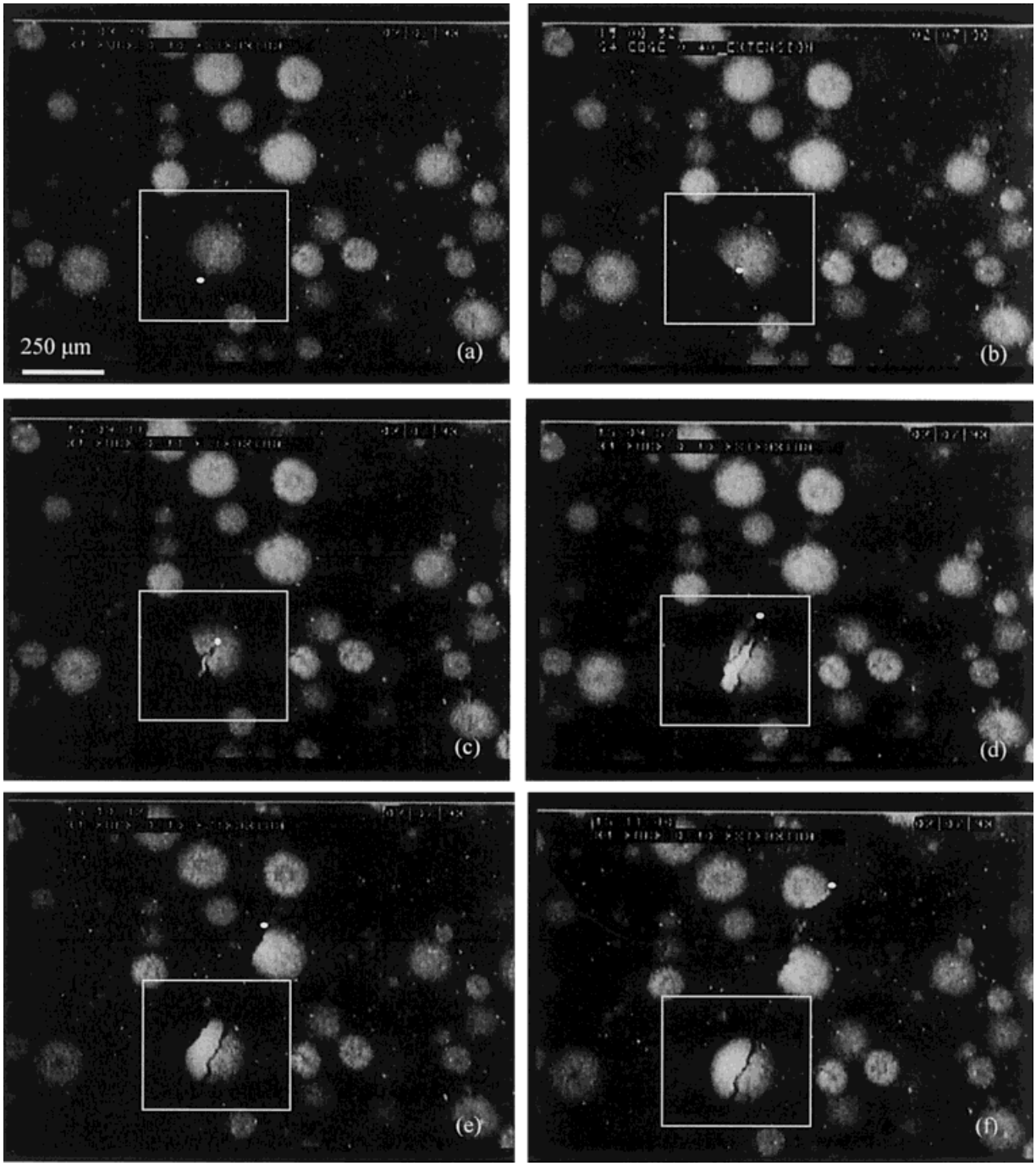

Figure 7 CLSM images of a notched CT test for composition V (slow cooling, large particles). Debonding of an included gelatin droplet in the continuous maltodextrin matrix is apparent. The bright spot corresponds to the crack tip, and the debonding event is highlighted with the white box.

continuous samples, which exhibited a very blunted crack tip morphology (reminiscent of ductile failure in metals); the tip morphology for the maltodextrin continuous composites was sharp (cf. ductile metals and brittle ceramics[18]). In Figure 7(a) the crack tip is close to a gelatin particle, which apparently remains unstressed compared to gelatin continuous samples.[7] In reality the crack tip was a region of stress concentration when the composite was under applied load (i.e.,

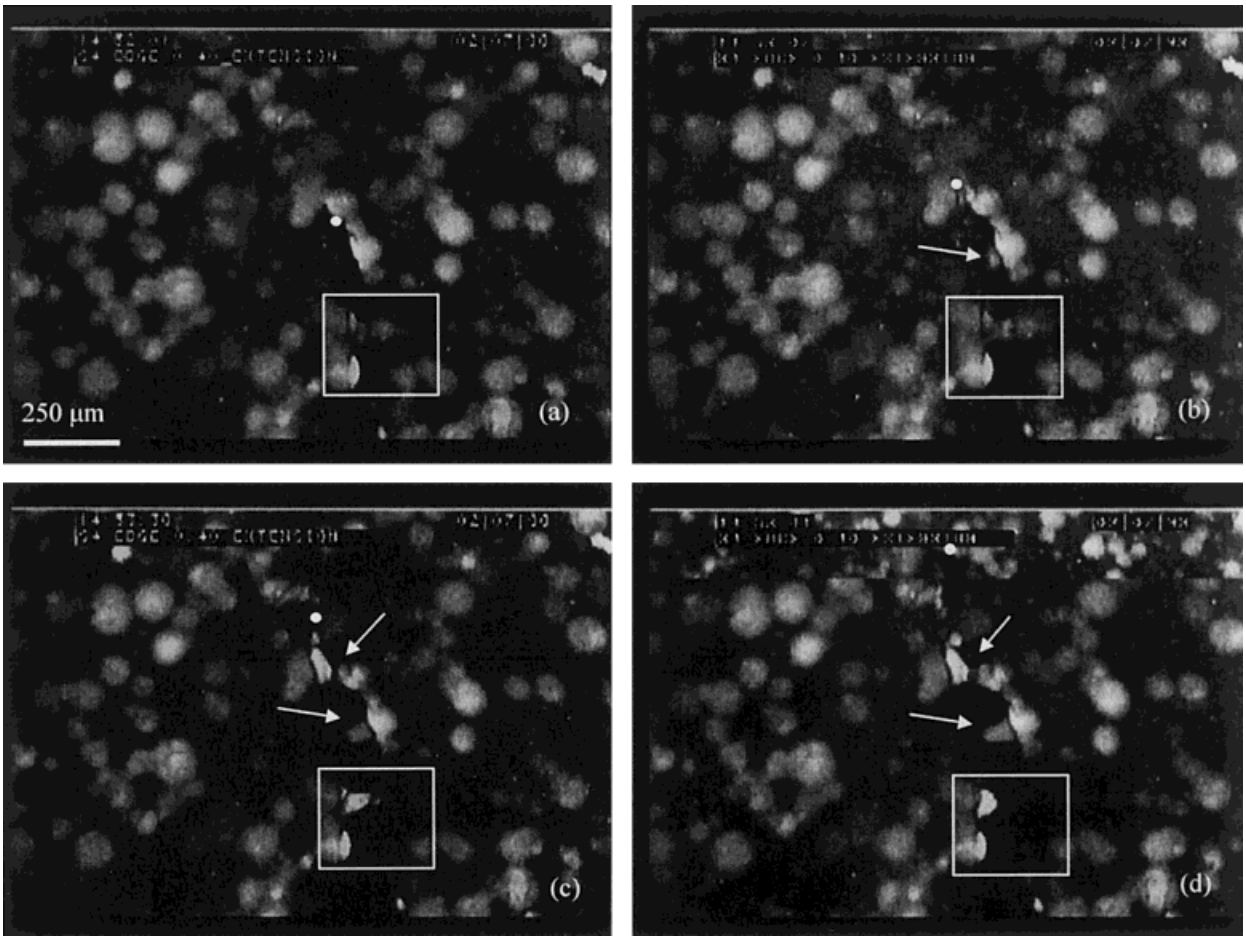

Figure 8 CLSM images of composition IV during the notched CT test (edge of the plate, small particles). In the insets there is (a) evidence of coalescence of gelatin particles, (b,c) gelatin ligament formation and stretching, and (d) relaxation after ligament pull-out. (b–d) Further ligament bridges are forming.

applied displacement). Further crack propagation [Fig. 7(b)] resulted in initial interfacial debonding between the spherical particle and the continuous maltodextrin matrix. This was revealed by a loss of contrast in the particle because air was present at the interface (shown in lower left side). In Figure 7(c,d) the crack propagates around the left side of the particle. As the crack advances further [Fig. 7(e,f)] the particle is totally detached from the matrix and pulled out of the left side of the crack, and a matching hole is retained on that side with the particle remaining "bonded" to the right side of the crack.

When the concentration of gelatin particles was higher, healing (or bonding) of neighboring particles occurred during gelation of the maltodextrin-rich matrix phase that occurred for some compositions after gelation of the particles. This is apparent in Figure 8(a,b), where crack propagation is retarded by ligaments of gelatin droplets bound to each other in the crack wake. This behavior may be viewed as a toughening mechanism for the brittle maltodextrin matrix (in a manner analogous to ductile metal toughened ceramics). Figure 8(a–c) shows a gelatin ligament that is stretched across the crack wake until it is finally pulled out from one side of the crack [Fig. 8(d)]. The strain in this ligament prior to pullout was significantly greater than 100%. In Figure 8(b) a new bridging ligament appears (white arrow), which is then followed by another one [Fig. 8(c)].

When a large notch was initially cut into the maltodextrin continuous samples, rapid sample fracture occurred. However, fine gelatin ligaments still bridged the crack with the sample being in two pieces. With such rapid failure of the sample in this instance it was impossible to de-

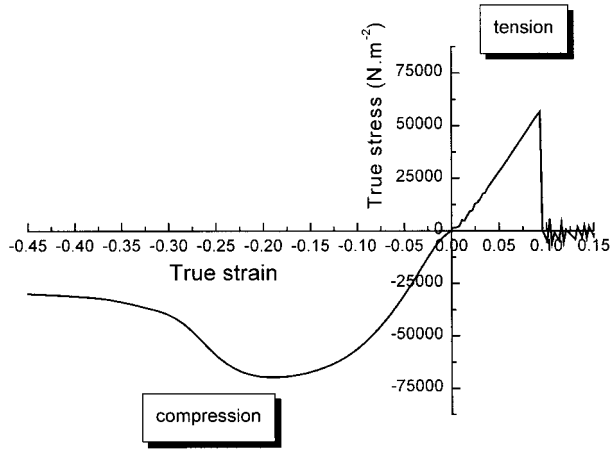

Figure 9 A comparison between tension and compression for a maltodextrin continuous sample with 33% included particles of the LH1e-rich phase. The true strain and stress were calculated according to eqs. (1)–(4).

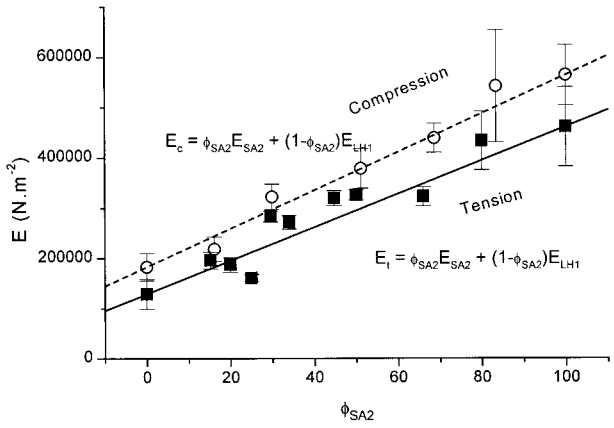

Figure 10 The Young's modulus evolution with the phase volume of the maltodextrin-rich phase and a comparison with the Isostrain model.

termine an accurate strain rate for the ligament deformation. However, with apparent strains of several hundred percent and failure occurring in less than 1 s, a strain rate in excess of 10^2 to 10^3 s^{-1} can be estimated. It is interesting to note that the strains observed in these ligaments were significantly higher than those noted during large deformation testing (under shear and compression) of pure gelatin, typically 150–200%.[19]

For deformation under compression, maltodextrin continuous samples did not exhibit ductile behavior, indicating that the matrix deformed and fractured before debonding between the gelatin particle and maltodextrin matrix could occur. However, as shown in Figure 9 for system VI (33% included gelatin phase volume), for a similar Young's modulus, fracture of the sample occurred under compression at a strain twice the value obtained under tension and for a stress value between 1.5 and 2 times the value obtained for tensile tests.

Effect of Phase Volume Fraction Ratios on Tension and Compression Failure Behavior

The effect of the phase volume fraction at constant phase composition was also investigated under compression and tension. Results were obtained for one tie line of the phase diagram, which corresponded to the 12% LH1e:12% SA2 in 0.1*M* NaCl system (III in Fig. 1). All composites were prepared by remixing the two separated phases to obtain the desired phase volumes, as described in the Experimental section. Therefore, the compositions and the characteristics of the two phases and the interfaces between the two phases were identical from one sample to another (assuming no water repartition on gelling), and only the phase volume and the particle size varied. The results found for the elastic moduli were consistent with the simple isostrain model,[20] whatever the nature of the continuous phase (Fig. 10).

The stress at failure as a function of the strain at failure for samples tested in tension and compression is shown in Figure 11. It can be seen that the strain at failure in compression was twice that in tension for all the samples. Compression tests may also be analyzed in terms of biaxial extension, the applied compression resulting in tension along the normal axes. For a material with a Poisson's ratio of 0.5, the tension strain

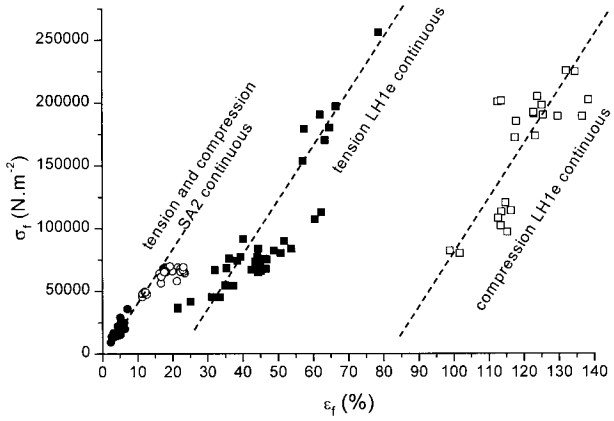

Figure 11 The envelope of failure for the composites: (●, ■) compression and (○, □) tension.

along the normal axes are half that applied in compression. The data shown in Figure 11 therefore suggests that the failure of the samples occurred in tension and that the Poisson's ratio of these materials was close to 0.5.

The stress at failure of the samples followed a different trend. For the maltodextrin continuous samples the stress at failure in compression was twice that of failure in tension. However, for gelatin continuous samples the stresses at failure in compression and tension were very similar. This may be explained by considering the failure of the samples to be strain dependent rather than stress dependent. For the maltodextrin continuous samples the stress increased linearly with the strain in tension right up until failure, so a doubling of strain led to a doubling of stress, which is evident in Figure 9 and reflected in the trend shown in Figure 11. However, for a gelatin continuous sample the stress varied little with strain above the yield point (Fig. 2); so if the strain was doubled the stress remained almost the same. Hence, in both systems the failure strain in compression was twice that in tension, and the difference in failure stress was merely a consequence of the different stress–strain functions.

However, the ϵ_f and σ_f fracture characteristics were strongly dependent on the continuous phase behavior and could not be treated directly as a function of the phase volume, because the nature of the matrix had an important influence (ductile when LH1e was continuous and brittle when SA2 was continuous). Therefore, two separated domains must be considered according to the composition of the continuous phase.

For a rubberlike matrix where filler spheres are embedded with no adhesion between the matrix and filler, Nielsen[21] suggested two fundamental relationships between the relative stress and the relative strain at failure with the phase volume of the filler:

$$\frac{\sigma_f(\text{filled})}{\sigma_f(\text{unfilled})} = 1 - \phi_{\text{filler}}^{2/3} \tag{5}$$

$$\frac{\varepsilon_f(\text{filled})}{\varepsilon_f(\text{unfilled})} = 1 - \phi_{\text{filler}} \tag{6}$$

In Figure 12(a,b) these formulas are applied for the gelatin-rich continuous composites. Unfortunately, according to this model, the size of the particle was not taken into account. The tendencies seen in these figures were however in good general agreement with eqs. (5) and (6), because the stresses and strains at failure decreased when the filler phase volume increased.

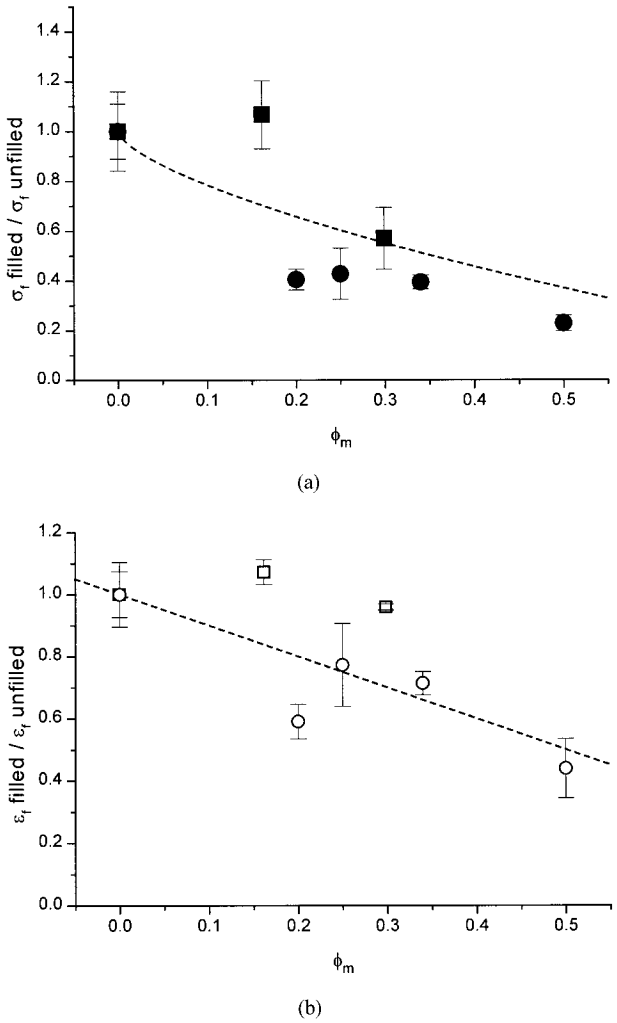

Figure 12 (a) The relative stress at failure as a function of the phase volume of filler for gelatin continuous composites: (■) compression, (●) tension, and (- - -) $1 - \phi_m^{2/3}$. (b) The relative strain at failure as a function of the phase volume of filler for gelatin continuous composites: (□) compression, (○) tension, and (- - -) $1 - \phi_m$.

For the maltodextrin continuous composites the tendencies were the opposite. When the phase volume of the gelatin increased, leading to greater cocontinuity of the structure, the strain and the stress at failure both increased. This phenomenon is largely believed to be due to the characteristics of the maltodextrin-rich matrix, which fails before any significant debonding can occur. It was therefore interesting to consider the effect of the presence of gelatin droplets in a maltodextrin matrix and, more particularly, on the work necessary to

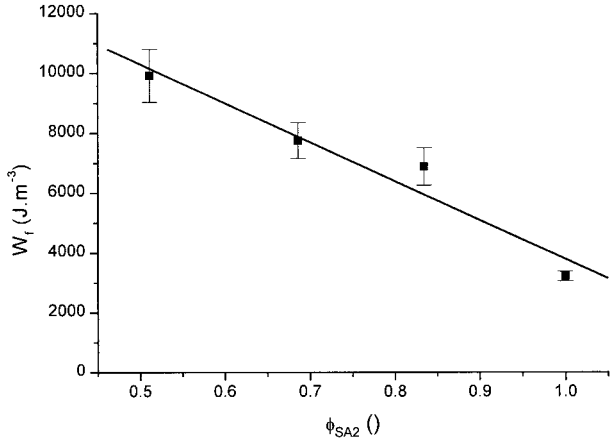

Figure 13 The work of fracture of the continuous phase as a function of the phase volume of the continuous phase for maltodextrin continuous composites.

break the matrix. The energy of fracture can be calculated by definition as follows[22]:

$$W_f = \int_0^f \sigma_i \, d\varepsilon \tag{7}$$

Even though the gelatin–maltodextrin interface is weak[7] and the fracture follows a route around the gelatin particles, the energy needed to fracture samples including gelatin particles *increases* with the phase volume of the gelatin (Fig. 13). A possible reason for the increase in the energy required for fracture is the energy required for deforming the bridging gelatin particles behind the crack tip (i.e., in the crack wake, see Figs, 7, 8).

CONCLUSION

The matrix–inclusion interface in gelatin–maltodextrin composites plays an extremely important role in their failure behavior. All samples prepared exhibited spherical inclusions of one phase embedded in a continuous matrix of the other. Gelatin continuous systems exhibited lower strength but were more resistant to fracture than the maltodextrin continuous systems (e.g., the elastic modulus was lower for gelatin continuous samples, but the failure strains were an order of magnitude greater). The shapes of the stress–strain (or load–displacement) curves were different, depending upon the continuous phase nature. The maltodextrin continuous samples were essentially brittle in nature, while the gelatin continuous samples exhibited a pseudo-plastic behavior (with an apparent yield stress). This latter phenomenon was attributed to interfacial debonding of maltodextrin particles from the gelatin matrix, which was observed when conducting dynamic tests on the CSLM microscope.

A comparison between compression and tension behavior was made and it highlighted the fact that the strain at failure in tension was twice as much as the strain at failure in compression. As a consequence, a Poisson ratio close to 0.5 was found, whatever the nature of the continuous phase in that system. The observed phase volume effect on the failure properties at a constant phase composition could correspond to the Nielsen model for nonadhesive filler particles in a rubberlike matrix, but improvement in this model is needed if the included particle size effect on the failure properties is to be described. Low adhesion between particles and matrix must be a criterion for a debonding phenomenon.

The authors would like to thank Dr. W. J. Frith and Prof. A. H. Clark for valuable discussions and comments.

REFERENCES

1. Kasapis, S.; Morris, E. R.; Norton, I. T.; Clark, A. H. Carbohydr Polym 1993, 21, 243.
2. Kasapis, S.; Morris, E. R.; Norton, I. T.; Gidley, M. J. Carbohydr Polym 1993, 21, 249.
3. Kasapis, S.; Morris, E. R.; Norton, I. T.; Brown, C. R. T. Carbohydr Polym 1993, 21, 261.
4. Kasapis, S.; Morris, E. R.; Norton, I. T.; Clark, A. H. Carbohydr Polym 1993, 21, 269.
5. Normand, V.; Pudney, P. D. A.; Aymard, P.; Norton, I. T. J Appl Polym Sci 2000, 77, 1465.
6. Loren, N.; Langton, M.; Hermansson, A. M. Food Hydrocolloid 1999, 13, 185.
7. Plucknett, K. P.; Normand, V.; Pomfret, S. J.; Ferdinando, D. P. Polymer 2000, 41, 2319.
8. van Vliet, T.; Walstra, P. Faraday Discuss 1995, 101, 359.
9. Ross-Murphy, S. B.; Todd, S. Polymer 1983, 24, 481.
10. Gao, Y. C.; Lelievre, J. Polym Eng Sci 1994, 34, 1369.
11. McEvoy, H.; Ross-Murphy, S. B.; Clark, A. H. Polymer 1985, 26, 1483.
12. McEvoy, H.; Ross-Murphy, S. B.; Clark, A. H. Polymer 1985, 26, 1493.
13. Brownsey, G. J.; Ellis, H. S.; Ridout, M. J.; Ring, S. G. J Rheol 1987, 31, 635.

14. Defloor, I.; Vandenreyken, V.; Grobet, P. J.; Delcour, J. A. J Chromatogr A 1998, 803, 103.
15. Durrani, C. M.; Prystupa, D. A.; Donald, A. M.; Clark, A. H. Macromolecules 1993, 26, 981.
16. Gent, A. N. J Mater Sci 1980, 15, 2884.
17. Bigi, A.; Bracci, B.; Cojazzi, G.; Panzavolta, S.; Roveri, N. Biomaterials 1998, 19, 2335.
18. Atkins, A. G.; Mai, Y. W. Int J Fracture 1986, 30, R49.
19. Bot, A.; van Amerongen, I. A.; Groot, R. D.; Hoekstra, N. L.; Agterof, W. G. M. J Chim Phys Phys Chim Biol 1996, 93, 837.
20. Takayanagi, M.; Harima, H.; Iwata, Y. Membr Fac Eng Kyushu Univ 1963, XXIII, 3.
21. Nielsen, L. E. J Polym Sci Polym Phys Ed 1979, 17, 1897.
22. van Vliet, T.; Luyten, H.; Walstra, P. In Food Colloids and Polymers, Stability and Mechanical Properties; Dickinson, E., Walstra, P., Eds.; Special Publication 113; Royal Society of Chemistry: Cambridge, U.K., 1993; p 175.